# Three-Dimensional Microstructural Characterization Using Focused Ion Beam Tomography

Michael D. Uchic, Lorenz Holzer, Beverley J. Inkson, Edward L. Principe, and Paul Munroe

**Abstract**

This article reviews recent developments and applications of focused ion beam (FIB) microscopes for three-dimensional (3D) materials characterization at the microscale through destructive serial sectioning experiments. Precise ion milling—in combination with electron-optic–based imaging and surface analysis methods—can be used to iteratively section through metals, ceramics, polymers, and electronic or biological materials to reveal the true size, shape, and distribution of microstructural features. Importantly, FIB tomographic experiments cover a critical size-scale gap that cannot be obtained with other instrumentation. The experiments encompass material volumes that are typically larger than 1000 $\mu m^3$, with voxel dimensions approaching tens of nanometers, and can contain structural, chemical, and crystallographic information. This article describes the current state of the art of this experimental methodology and provides examples of specific applications to 3D materials characterization.

## Introduction

The importance of material microstructure and its subsequent influence on properties is a basic tenet of materials science. Therefore, one might reasonably expect to find a suite of mature materials characterization methodologies that provide an unbiased, accurate, and complete description of microstructural features at length scales over which microstructural features are generally observed, i.e., from nanometers to millimeters in size. Unfortunately, this is often not the case. Many commonly used characterization methodologies at the microscale, such as scanning electron microscopy (SEM), electron backscatter diffraction (EBSD), energy dispersive spectroscopy (EDS), and scanning probe microscopy and its derivatives such as atomic force microscopy, all provide near-surface information but cannot inform the user about the exact nature of microstructural features except in selected cases where the feature geometry is symmetric, highly idealized, or *a priori* known. To achieve truly quantitative materials characterization, it is imperative that modern characterization methodologies provide three-dimensional information.[1] Specifically, 3D characterization enables the measurement of a number of important geometric properties that cannot be obtained using a 2D analysis, such as the number of features per unit volume, feature connectivity, real feature shapes and sizes, and spatial distribution information.[2]

One well-established method for obtaining 3D information from instruments that only provide 2D data, such as those listed above, is by serial sectioning.[2] Serial sectioning experiments are conceptually simple. The first step is to create a planar surface through careful removal of a known volume of material. This process is typically accomplished via mechanical sectioning, mechanical grinding and polishing, or ion milling. After sectioning, the freshly exposed surface is analyzed using a variety of 2D characterization methodologies; this process of sectioning and imaging is repeated until the desired material volume is interrogated. After the experimental data acquisition is complete, this information is reconstructed and analyzed using image processing and visualization software. This type of 3D characterization is also referred to as tomography, which is defined as imaging by sections, or sectioning.

Serial sectioning tomographic experiments are most commonly performed at the macroscale using mechanical polishing and optical or scanning electron microscopy,[3–5] and there are a number of variations that use alternate approaches tailored to both organic[6,7] and inorganic materials.[8,9] One of the most important considerations for serial sectioning experiments is the depth of removal between sections, which must be a relatively small fraction of the dimensions of the features of interest to obtain a high-fidelity representation of those features. A general rule is that a minimum of 10 sections per feature is needed to accurately characterize feature size and shape. Also, in order to produce 3D reconstructions that have minimal distortions, it is preferable to have the sectioning depth be of similar size to the in-plane resolution of the characterization system. Given that there are many microstructural features that are micron or submicron in scale, the study of these features in 3D requires the use of highly precise sectioning capabilities.

The advent of focused ion beam (FIB) and FIB–SEM instruments has enabled serial sectioning tomography experiments to be scaled to study micron-scale and smaller features.[10–15] These microscopes have the ability to focus highly energetic ions (typically 30 kV $Ga^+$) to extremely small spot sizes—on the order of 5–20 nm. This small spot size in conjunction with rastered movement of the ion beam enables the controlled removal of material at the nanoscale via ion sputtering interactions. These instruments feature unrivaled precision for machining a series of parallel surfaces. Specifically, these microscopes are able to control the average serial

sectioning depth to a minimum value of approximately 10–15 nm using appropriate control measures.[16,17] This value is at least an order of magnitude finer than what traditional mechanical sectioning methods can accomplish.[3,18]

It is important to note that FIB milling has some additional positive attributes relative to the task of serial sectioning. First, ion milling is a fairly universal method for micromachining. Planar, smooth surfaces have been successfully prepared by cross-section FIB milling for metals, ceramics, polymers, and electronic and biological materials. Arguably there is no other sample preparation method that works as well with this diverse set of materials. Second, the method results in relatively low damage as compared with typical abrasive or cutting methods; this preserves the true microstructural form, especially for materials that are composed of both soft and hard phases or that contain significant porosity. Last, the material removal rates are sufficient for serial sectioning experiments at the microscale.

One other significant feature of FIB and FIB–SEM microscopes is the potential incorporation of a number of high-resolution imaging and surface analysis methodologies, such as backscattered electron (BSE) imaging, secondary electron (SE) imaging, ion-induced secondary electron (ISE) imaging, EBSD, EDS, Auger spectroscopy, and secondary ion mass spectroscopy (SIMS). The information limits for these methods are typically of the same order of magnitude as the FIB sectioning capabilities.

For microscopes that contain many of these characterization systems, the ability to acquire chemical, crystallographic, and/or structural information provides the user with tremendous flexibility to select which types of information are important for their particular study. For example, if only structural information is required, then it is likely that image data will suffice to characterize microstructural features, where both imaging modes and contrast levels are optimized to assist with feature segmentation. Chemical or crystallographic analysis can be included to help this process or, more likely, are obtained to provide additional information about the local nature of microconstituents.[19–23]

The purpose of this article is to provide an overview of recent developments and applications of FIB microscopes for 3D materials characterization at the microscale. The experiments usually encompass material volumes that are typically larger than 1000 μm$^3$ with voxel dimensions approaching tens of nanometers. Notably, this combination of spatial coverage and resolution (Figure 1) cannot be achieved with any other instrumentation.

Next, we briefly describe the typical experimental procedure for data collection, followed by selected examples of applications of this state-of-the-art 3D materials characterization methodology.

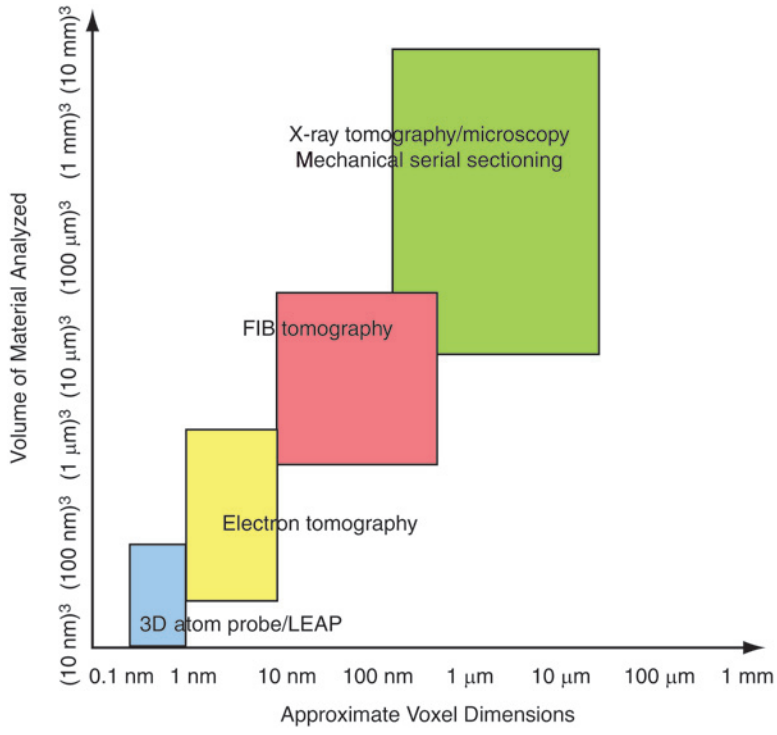


Figure 1. Graphical representation of the resolution and typical volume analyzed per experiment for modern tomographic characterization methods. The focused ion beam (FIB) and FIB–scanning electron microscopy (FIB–SEM) tomography experiments cover a critical length-scale gap and are ideally suited for 3D characterization of submicron- and micron-sized microstructural features. LEAP is local electrode atom probe tomography.

## The Experimental Procedure and Data Processing

### *Data Acquisition*

FIB tomographic experiments have been performed with both single-beam and FIB–SEM (dual-beam) instruments. The distinction is somewhat historical. Single-beam microscopes have been commercially available for more than 20 years, whereas FIB–SEMs have only been produced for materials science laboratories in the last few years. Thus, early demonstration of this methodology used single-beam FIB microscopes,[10–15,24] whereas later examples used FIB–SEMs.

For most tomography experiments, the FIB is used to prepare a new section using cross-section milling, where the ion beam is oriented parallel to the sectioning plane of interest.[13–15,24] Figure 2a illustrates this standard sample geometry relative to the electron and ion beams for an FIB–SEM. Cross-section milling is almost always used because this beam-to-sample geometry produces nominally flat surfaces, even when the milling rates of various microconstituents are vastly different. Differential milling is usually observed in polyphase and polycrystalline materials, because milling rates are dependent on a number of factors that include chemistry, crystallographic orientation, and surface topology.[25] Direct normal milling, where the ion beam is at normal incidence to the sectioning plane, has also been used for FIB tomography experiments[26,27] and is sometimes referred to as depth profiling in the surface analysis community (this type of experiment is commonly performed using SIMS). However, one has to be careful, when using this methodology, that the sectioning plane remains planar during the experiment, because of the aforementioned sensitivity of milling rates to surface topology, and there can be other geometrical constraints that limit the overall utility of depth profiling.

The typical procedure for performing an FIB tomography experiment using cross-sectioning milling is outlined as

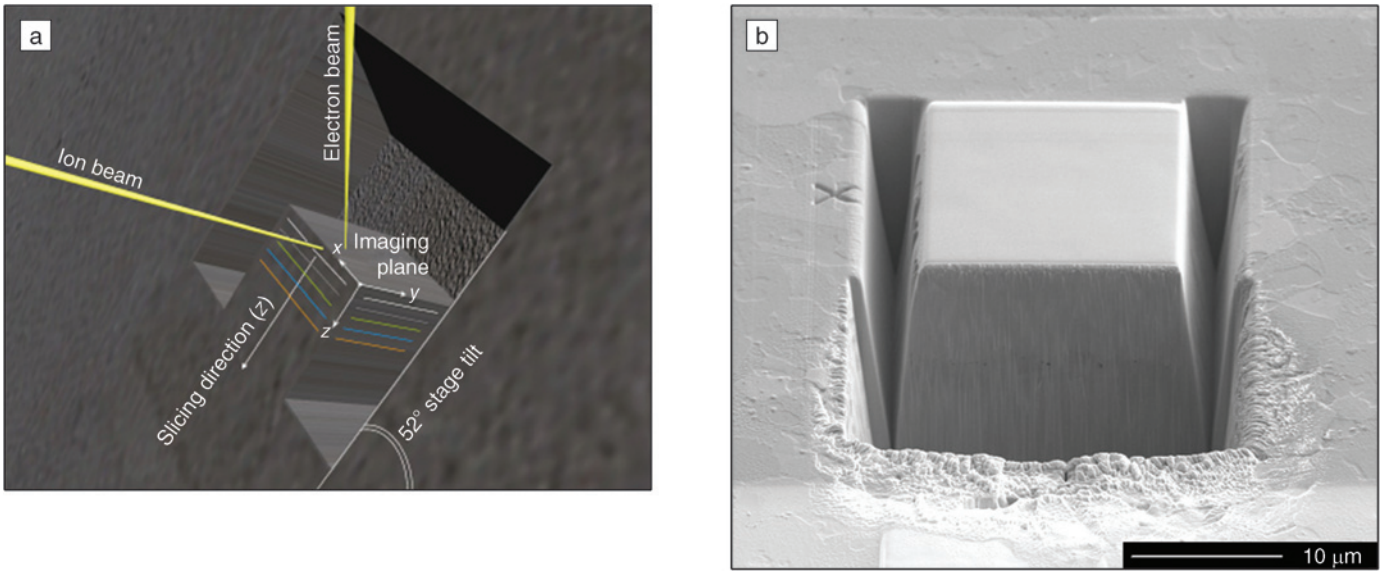


Figure 2. (a) Typical sample geometry and beam orientation for a FIB–SEM tomography experiment using cross-section milling.[16] (b) Secondary electron image of a volume of material prepared for serial sectioning analysis.

follows. First, an area of interest is located on the surface of a bulk sample, and the FIB is used to create a trench around this area with high beam currents (5–20 nA). The dimensions of the trench are dictated by a few factors. The trench geometry should allow for cross-sectioned surface imaging at an oblique angle with either the electron beam or the ion beam.[13–15] The trenches to either side of the volume of interest must be large enough to prevent significant redeposition of sputtered material back onto the cross-sectioned surface, eliminate shadowing of imaging signals that cause intensity variations that make image segmentation difficult,[16] and remove material that blocks access to other analysis methods such as EDS[19] or EBSD. Other sample geometries can be used to further maximize the ability to access signals from the entire cross-sectioned surface and eliminate redeposition effects.[22] A protective platinum film, typically about 1 μm thick, is usually grown using FIB-induced decomposition of precursor gases on the top surface of the volume of interest before trenching to prevent unwanted milling or $Ga^+$ implantation in this surface. The protective cap can also minimize small ripples on the cross-sectioned surface that are caused by sharp changes in the topology of the top surface, which are colloquially referred to as "waterfalls" or "curtains."[25] Fiducial markers are often milled on the top surface of the volume of interest as well. Fiducial markers are independent reference features for image alignment/registration of the series of 2D images into a 3D data array[13–15] and are also useful for instrument automation.[16,22,23]

After these steps are completed, the serial sectioning experiment can begin. Typical ion beam currents for serial sectioning are usually between 30 and 1000 pA; the selection of a specific beam current is usually a tradeoff between the ion beam spot size, which can influence factors such as the minimum sectioning depth, surface roughness, and taper of the sectioned surface, and the time needed to complete the sectioning process. The current and milling time of the ion beam are selected to ensure that each cross-section mill cuts completely through all materials to the desired depth. Typically, the calculation of milling time is based upon a computer materials file that has been derived from measured or theoretical values input by the user.

Note that the thin damage layer created by $Ga^+$ ion implantation during FIB milling is usually not an issue for ISE, SE, or BSE imaging but can be a problem if the material is sensitive to ion beam damage or if a specific analytical method requires low-damage surfaces. For example, the damage layer can affect the collection of EBSD data; this is discussed later. A lower FIB voltage will reduce the depth of the damage layer, whereas a reduced milling current may also help reduce the level of damage, particularly on organic or biological specimens.

Once the sectioning process is completed, an image of the as-sectioned surface is collected or other surface analysis is performed. In single-beam FIB microscopes, this requires moving the sample stage to expose the freshly milled surface to the ion column to collect an ISE image.[10–15,24] For FIB–SEM microscopes, the sample does not need to be moved in order to collect a SEM image if the sample is placed at the height where both electron and ion columns can simultaneously image the same area of the sample. Thus, FIB–SEMs offer a simpler approach to the standard experimental procedure of cutting and imaging. Some FIB–SEMs even allow for simultaneous operation of the SEM during the FIB milling process, which can produce extremely high-density data sets containing both SE and BSE images while reducing the time needed for data collection.[28]

In addition to image data, if the trench surrounding the sample volume provides adequate clearance, EDS maps can be collected as well without moving the sample.[19] However, the usual position of EBSD detectors for commercial FIB–SEMs requires sample movement to collect crystallographic data.[20–23]

An important aspect of the conceptual design of FIB–SEM tomography studies that are truly nanoscale, that is, the in-plane pixel resolution and serial sectioning depth have dimensions on the order of 10–20 nm, is consideration of the information limit for a particular characterization

methodology. For electron imaging at these small dimensions, there are many aspects regarding the electron interaction volume and the type of electron detector used that can affect the resolution of a particular imaging condition. These parameters should be adjusted such that the information limit for the imaging mode is smaller than that for the minimum voxel dimension to eliminate the possibility of collecting data that has "empty magnification."

One final development of note in the past few years with regard to FIB–SEM data collection is the implementation of automation control scripts. Automation is an essential aspect of serial sectioning devices, as the iterative nature of the experiment is ideally suited for autonomous computer control. In their most basic form, these scripts perform the primary functions of cross-section FIB milling of the sample and SEM image collection, which provides a more consistent serial slice thickness, reduces the time needed per acquisition cycle, and enables the microscopes to run unattended for relatively long periods of time.[29] More advanced control scripts incorporate image recognition procedures to minimize the effects of electrical, thermal, or mechanical drift[16] or to incorporate a wider range of data signals, which requires accurate sample repositioning after complex stage movements.[22,23]

### *Data Processing and 3D Reconstruction*

After collection of the experimental data, which can consist of a series of SE images, BSE images, ISE images, EBSD maps, EDS maps, and so on, the data are usually reconstructed into a 3D volume for visualization purposes or for further analysis. For most experiments, the series of 2D data files must undergo some signal processing before these can be input into visualization and analysis packages. There are many commercial and freeware software packages to assist with this process, and most FIB microscope manufacturers now offer signal processing and visualization software as part of their serial sectioning analysis packages.

A typical sequence for data post-processing is as follows. First, the individual 2D data files are aligned with respect to each other, as most FIB tomography experiments produce data that contain both systematic and random translations between consecutive sections. These corrections can be done manually or automatically using signal processing algorithms such as cross-correlation. This process is often assisted by using only subregions of the original data that contain fiducial markers, which provide an independent reference for registration. Also, any distortions in the physical dimensions of the data array should be removed.

One frequent distortion in FIB–SEM tomography is the foreshortening of SEM images. Here, the sample geometry relative to the instrument frame (Figure 2a) is such that the normal of the as-sectioned surface is at an oblique angle relative to the electron column, and therefore the scale of the image in the vertical direction must be corrected for projection effects. Foreshortening corrections are often performed in single-beam FIB experiments as well because of sample stage movement limits.[13–15,24] Another common correction is to further adjust the dimensions of the 2D in-plane data through interpolation routines to match the out-of-plane distance between consecutive sections in order to produce cubic voxel arrays. Last, a subregion is usually cropped out from the 3D data set to define a volume that removes artifacts from the data set, to eliminate areas that have poor data quality, and, if needed, to minimize the data volume size to prevent problems with computer memory allocation.

After the image alignment and voxel regularization steps are completed, the voxels of the data set are classified as belonging to a particular microstructural feature or group of features for most visualization and analysis studies; this procedure is often referred to as data segmentation. This process can be extremely easy or impossible at times and is wholly dependent on the type, quantity, and quality of data from the FIB tomography experiment.

For example, consider a two-phase microstructure that consists of a matrix phase and precipitates that are well separated from each other. If obtained images of this structure show a large contrast difference between the two phases and the contrast/brightness levels are maintained throughout the experiment, data segmentation might consist only of a threshold operation. Unfortunately, the complexity found in most microstructures and/or the experimental data limitations often make life more difficult. There are a number of resources on signal processing filters as well as examples where these filters were successfully applied to microstructural image data.[30,31] Analysis of crystallographic or chemical maps rather than image data can alleviate some of these difficulties,[19,23] and there is no substitute for optimizing image modes and contrast levels to aid this process.[30] However, for many studies, robust data segmentation is the most problematic and rate-limiting step for performing 3D visualization and analysis.

The remainder of this article provides three examples of applying FIB and FIB–SEM microscopes to characterizing micron and submicron features in a variety of materials systems. The reader is also referred to a number of additional studies that perform similar (or demonstrate the feasibility of) FIB tomographic experiments, such as the study of 3D feature morphology of microelectronic or thin-film structures,[17,32,33] fuel cells,[34] ceramics,[16] biological materials,[35,36] porous rocks,[37] and nanoindentations in multilayer[15] or amorphous carbon films;[38] 3D x-ray spectral analysis of precipitates and corrosive products in metallic alloys;[19] and the mapping of internal orientation gradients underneath nanoindentations[20] or around hard precipitates.[21]

## Example 1: Single-Beam FIB Tomography

One of the most obvious applications of tomography is to characterize the true shape and distribution of microstructural features. Historically, it has been very difficult to analyze, in 3D, extremely localized features such as cracks, anomalous grains, residual wear damage, and failure sites, because of problems in locating and sampling such features. A key driving force for developing FIB tomography is its potential to analyze such features in 3D because of the great spatial accuracy with which the ion beam can be positioned.

The 3D shape and spatial distribution of cracks is extremely important in many nanotribology materials problems. For this first example, a quantitative characterization of the size and distribution of subsurface cracks produced during frictional wear of a sharp diamond stylus against the surface of an alumina and alumina-5 vol% SiC nanocomposite was carried out.[24] Previous studies showed that the nanocomposite exhibited significant improvement in contact wear resistance relative to the pure alumina, and this effort sought to quantify the role that the nano-sized SiC particles played in the development of residual damage. Note that the experimental approach used in this study, cross-section milling and imaging using only an FIB column, was also used to quantify the 3D morphology and volume of individual grains in an extruded FeAl intermetallic alloy[14] and to quantify in 3D the deformed substructure and pile-up of multilayered thin films underneath nanoindentations.[13,15]

Some details of the FIB tomography experiment are as follows. The FIB was used to locate a wear track on the surface of a bulk sample and create a large trench that was oriented perpendicular to the wear track, so that the cross-section profile of the wear track could be viewed with ISE imaging after tilting the sample. Reference markers consisting of a series of small holes were milled into the top surface of the sample to assist with image alignment. The serial sectioning experiment used a 500 pA beam to perform the cross-section milling that exposed a new surface for imaging and a 50 pA beam to collect ISE images both along the FIB milling direction (to measure the depth of material removal for that particular section) and at a sample tilt of 45° to image the as-sectioned surface.

For this experiment, a reasonably low magnification of 15,000× was chosen to enable the field of view to encompass the entire width of the scratch track and observable crack field, shown in Figure 3a for the alumina and nanocomposite materials. Because alumina is slow to sputter, relatively wide sectioning separations (300–600 nm) were used as a compromise between experimental time and accuracy (sufficient sections to accurately sample the cracks).

The crack profiles appear as dark lines in the ISE images because of reduced secondary electron yield as compared with the matrix. Data segmentation was performed using a threshold operation, and the determination of the crack profiles sometimes required contrast enhancement using edge filters or manual adjustments. All signal processing, data segmentation, and 3D visualization was performed using Interactive Data Language (Research Systems Inc.). Cumulative minimum errors in the 3D location of the crack relative to the wear track surface (arising from registry and segmentation errors) were between 3 and 5.8 pixels, equivalent at the 15,000× magnification (23 nm pixel size) to be +115 nm and +135 nm within the 2D sectioning plane, and +70 nm in the sectioning direction.

Figure 3b shows 3D reconstructions of the crack zones as viewed "inverted" (from inside the sample). In these reconstructions, the scratch tracks are shown as gray solid surfaces at the bottom of each image, and the cracks are shown as white features on a black background. See Reference 24 for a discussion of the labels A–F in Figure 3b, which denote specific microstructural regions around and underneath the wear track. The dimensions of the reconstructions shown are 19.1 μm across the scratch and 7.2 μm along the scratch profile for the alumina sample, and 16.8 × 4.3 μm for the nanocomposite. The FIB tomography experiments provided unique quantitative evidence that both the alumina and nanocomposite exhibited similar 3D crack distributions that were composed of three zones: the first was directly underneath the wear track and was deficient in cracks, the second surrounded the first zone (extending up to the surface) and contained a high density of microcracks, and the third was below the other zones and was composed of deep lateral and median cracks that did not extend to the surface. The tomographic data also enabled the observation of crack deflection or pinning around the nanocrystalline SiC particles that were observable in the ISE images (>30 nm) of the nanocomposite. In short, the use of 3D tomographic analysis enabled the quantitative identification and measurement of crack distributions and qualitative 3D views of crack morphologies that were not obtainable using conventional micro-imaging methods.

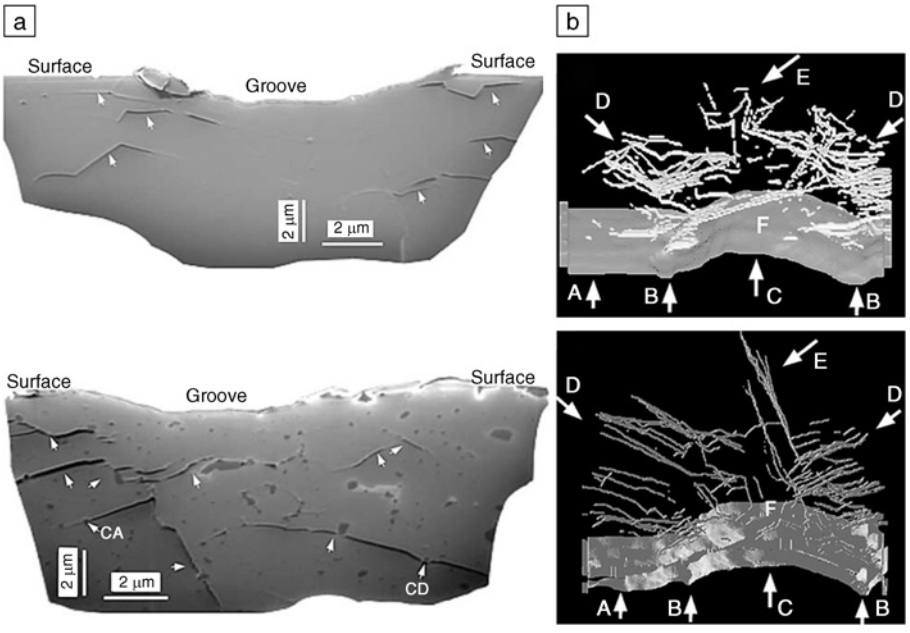


Figure 3. (a) Ion-induced secondary electron images of crack formation below a wear surface for alumina (top) and alumina-SiC nanocomposite (bottom).[24] Arrows in the images point to major subsurface cracks. (b) 3D reconstructions of the cracks generated around a scratch track, viewed "inverted" (from inside the sample), for alumina (top) and nanocomposite (bottom). See Reference 24 for a discussion of the labels A–F in (b), which denote specific microstructural regions around and underneath the wear track.

## Example 2: FIB–SEM Tomography

This next example demonstrates the use of 3D FIB tomography to quantitatively characterize the true size and shape of portland cement grains in an agglomerated state.[39,40] This study was motivated by the lack of high-resolution 3D characterization data of fine cement particles, needed as input data for modeling of rheological and hydration processes.[41,42] In particular, modern predictive models are now able to use more realistic depictions of granular microstructures rather than idealized representations of spheres and ellipses. The fidelity of these property models is thought to depend not only on the quality of the physical laws that describe particle interactions, but also on the quality of the characterization and 3D representation of realistic particle morphologies.

For these models, characterization of the fine particle size and distribution in portland cement is very important, as 90% of the internal surface area is formed by cement particles <10 μm in size. A major challenge for statistical particle analysis from cement powders is reliable object recognition, because fine, submicron-sized cement particles tend to form agglomerates even under dry storage conditions. High-resolution 3D imaging capability in combination with sophisticated image analysis is therefore a prerequisite for geometrical characterization of individual subgrains from within the

agglomerates. For this purpose, FIB tomography opens new possibilities to characterize complex, fine-grained particulate systems.[39] Furthermore, specially tailored computational approaches for particle recognition and stereological correction of boundary truncation effects have been presented for the extraction of quantitative microstructural parameters from the FIB data volumes.[40]

The analysis was performed on five different grain size fractions from portland cement (CEM I 42.5), ranging in median size from 0.91 to 14.2 μm. The dry compacted cement powders were impregnated with a low-melting-temperature alloy (Wood's metal, an alloy composed of bismuth, lead, tin, and cadmium) to increase contrast between the pore structure and the cement particles and reduce charging effects, both of which greatly aided the automated segmentation of the cement particles. An FIB–SEM microscope was used, which enabled the stage to remain stationary during the experiment (in contrast to the previous example), and data collection comprised a series of SE images. The elimination of mechanical stage movements and the use of custom microscope control scripts that employed drift-correction measures provided much higher precision of the serial sectioning depth.

Using this methodology, a minimum sectioning depth of 15 nm could be reliably achieved using a 50 pA beam current. However, many of the tomography experiments did not require this fine sectioning depth; one objective of this study was to tailor the sectioning depth to the in-plane pixel resolution of the SE images to have nominally cubic voxels that provided accurate data analysis in 3D space.

The FIB–SEM microscope used in this study had maximum image resolution limitations (a maximum value of 1024 × 884 pixels), and therefore the size scale of the median particle size dictated the appropriate sectioning depth. As a result, the five data volumes were collected for a range of resolutions and size scales. For the smallest median particle size of 680 nm, the average voxel dimension was approximately 12 nm, and the volume encompassed $5 \times 5 \times 3$ μm, whereas for the largest median particle size of 14.2 μm, the average voxel size dimension was approximately 116 nm and the total volume encompassed $65 \times 46 \times 34$ μm. The proportionally large data volumes contained between 1200 and 3800 particles, enabling statistical analysis of the microstructural data. Preprocessing of the image data after the experiment consisted of leveling the background contrast and image registration. An automated analysis of the intensity histogram was used to segment the ceramic particles from the metal matrix, and a refined 3D watershed algorithm was developed to define boundaries between agglomerated particles. In addition, truncation effects at the data volume boundary must be corrected with stereological procedures in order to obtain accurate statistical particle analyses.[40] All signal processing algorithms were developed using Matlab 7.0 (MathWorks), and 3D visualizations were performed with Amira 3.1 (Mercury Computer Systems Inc.).

The 3D reconstructions of the five data volumes are shown in Figure 4a, where the data segmentation process has identified each particle and assigned it a different color. This figure clearly shows the ability of FIB–SEM microscopes to characterize submicron and larger microstructure features for a range of length scales and to provide high-fidelity representations of the surface topology. Subsequent shape analysis of the 3D moments of inertia for each particle showed that the average moment of inertia was similar for all five particle size classes studied (i.e., no size dependency of shape was observed). Another representation of the data is shown in Figure 4b, which highlights the ability of 3D FIB tomography to observe the fine details of microstructural features. The images on the left side of Figure 4b show a region of agglomerated particles that form a dense intergrowth; the images on the right show a strongly fragmented domain where a larger particle has disintegrated into numerous subgrains. The scale of these structures is such that methods such as x-ray tomography or mechanical serial polishing could not resolve the finest microstructural features and likely would interpret the agglomerated objects as a single feature, and the analysis volume would well exceed the capabilities of nanoscale 3D characterization methodologies such as TEM tomography and atom probe tomography.

## Example 3: FIB–SEM and EBSD Tomography

This final example illustrates the use of the FIB–SEM and EBSD to characterize the 3D grain structure of a polycrystalline Ni superalloy.[22,23] The motivation for this study was similar to the previous example, which was to provide unbiased, quantitative, and high-fidelity descriptions of grain-level microstructural features for modern mechanical property prediction programs.[43] These descriptions might consist of either direct or synthetic representations of microstructures in 3D or a series of statistical functions that describe microstructural feature distributions such as the grain volume, number of nearest neighbors, grain shape, and orientation information.[23]

The majority of the grains in this material range in size from 2 to 5 μm in diameter, so a sectioning depth of ~200 nm is sufficient to characterize grain morphology. Previous FIB tomography studies of this material were successful in collecting image data of the grain-level microstructure, but subsequent data segmentation of the grain-boundary network proved difficult using either SE or ISE images. A representative ISE image of the engineering alloy IN100 is shown in Figure 5a, which highlights the complexity of its microstructure. Therefore, EBSD diffraction patterns were collected to enable fully unsupervised segmentation of the grain-level microstructure. It is beyond the scope of this article to fully describe the EBSD technique, and the interested reader should consult references for further study.[44] To generate an EBSD pattern, an incident electron beam forms an angle of approximately 20° with the sample surface. The glancing-angle geometry of the electron beam facilitates production of electron channeling patterns (commonly called electron backscatter diffraction patterns), which escape from the near-surface region of the sample and are collected via a phosphor screen and charge-coupled device camera. Collectively, EBSD patterns contain local information about crystal structure and orientation and are sensitive to strain and lattice deformation. The spatial resolution of the technique is on the order of 10–20 nm under ideal conditions, whereas the depth resolution is material-dependent and on the order of 30 nm.

Issues related to surface damage and sample geometry must be addressed to incorporate EBSD mapping in the serial sectioning experiment. As mentioned previously, surface preparation is typically more stringent for EBSD analysis than for the two previous examples, where the experiments consist only of electron or ion imaging. This is because the quality of EBSD patterns is highly sensitive to the degree of surface damage. Ion milling is known to produce a thin amorphous or highly defected layer caused by ion implantation effects; the thickness of this layer is dependent on a number of factors including material chemistry, crystallography, accelerating voltage, and incident angle of the ion beam. Good EBSD patterns have been obtained with 30 kV $Ga^+$ prepared surfaces for metals such as Cu,[20] FeAl,[21] and Ni alloys,[22,23] but this condition is not always observed.[45]

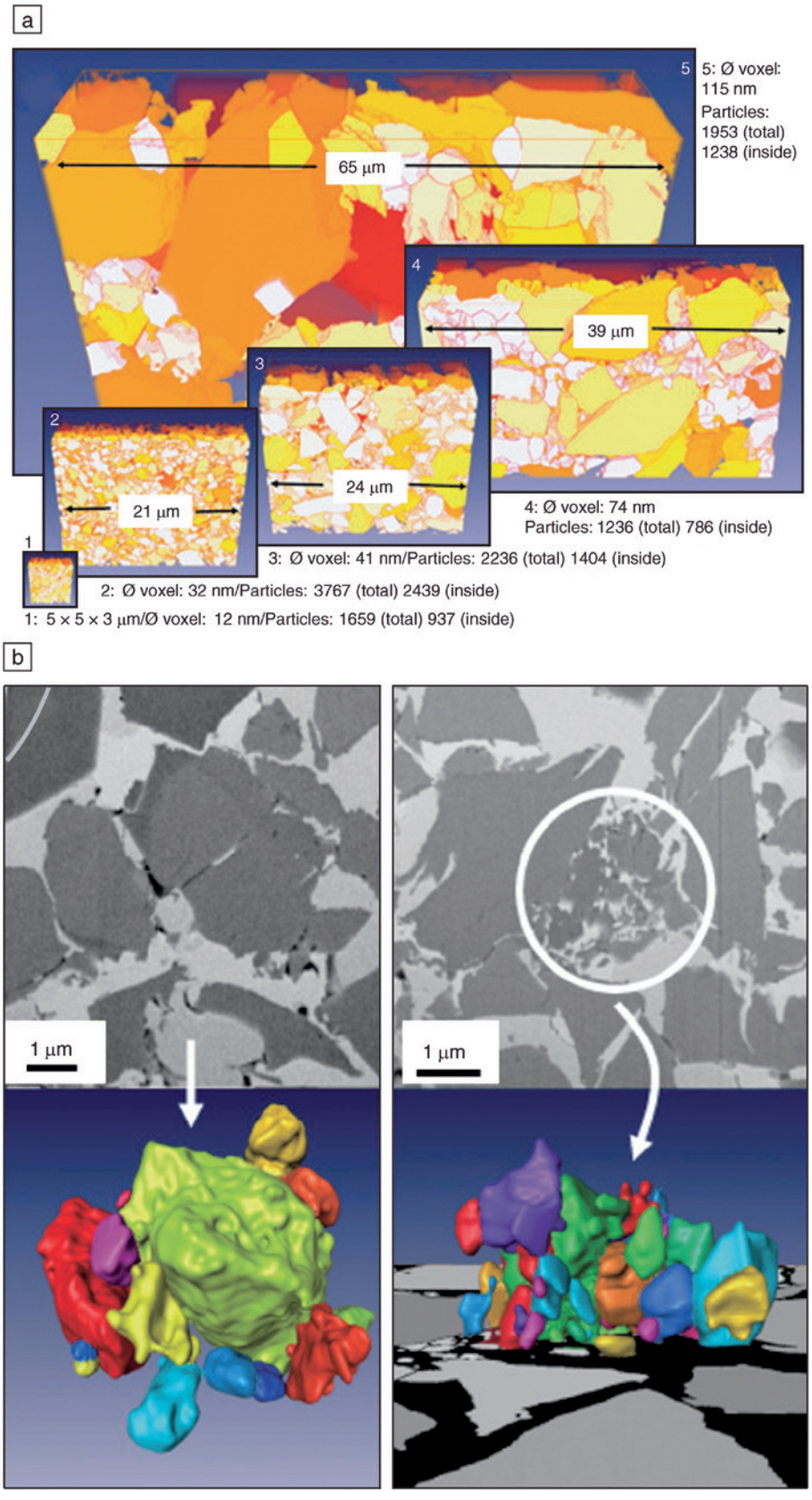


In addition to surface preparation issues, EBSD patterns can only be collected if there is a line of sight from the sample surface to the EBSD camera system. One way to meet this requirement is to place the volume of interest at the edge of a bulk sample.[19–22] If the volume of interest is located within the interior of a bulk specimen, only a very small area from the top of the cross-section surface will have an observable EBSD pattern, and the rest will be blocked by the sample unless very large trenches are made.

The full details of the FIB–EBSD tomography experiment can be found elsewhere[22,23] and thus will only be discussed briefly here. As mentioned earlier in this section, a preferred sectioning depth for this sample would be ~200 nm, based on the typical range of grain sizes. A sectioning depth of 250 nm was selected as a compromise value because of time constraints and enabled the sectioning depth and the in-plane resolution of the EBSD map to be equivalent. The experiment comprised moving the sample repeatedly between two microscope stage positions: the sectioning position and the EBSD mapping position. Similar to the previous example, custom microscope control scripts that use image recognition were developed for precise and automated alignment of the sample between the two stage positions. When the sample was in the sectioning position, the FIB was used to mill a cross-section surface using a 3000 pA beam. After sectioning, the sample stage was rotated and translated to bring the cross-section surface into the EBSD analysis position, and an EBSD map and four ISE images (which were not used in this example) were collected for each section before returning to the sectioning position.

Preprocessing of the EBSD data after the experiment consisted of a rough alignment step, after which the series of 2D

Figure 4. (a) 3D reconstructions of portland cement particles.[39,40] The reconstruction dimensions, average voxel dimensions, and number of particles per data set are listed on the figure for each data set. (b) Two secondary electron images (top) and corresponding 3D reconstructions (bottom) that show the fine details of microstructural features. The images on the left side show a region of agglomerated particles that form a dense intergrowth; the images on the right show a strongly fragmented domain where a larger particle has disintegrated into numerous subgrains.

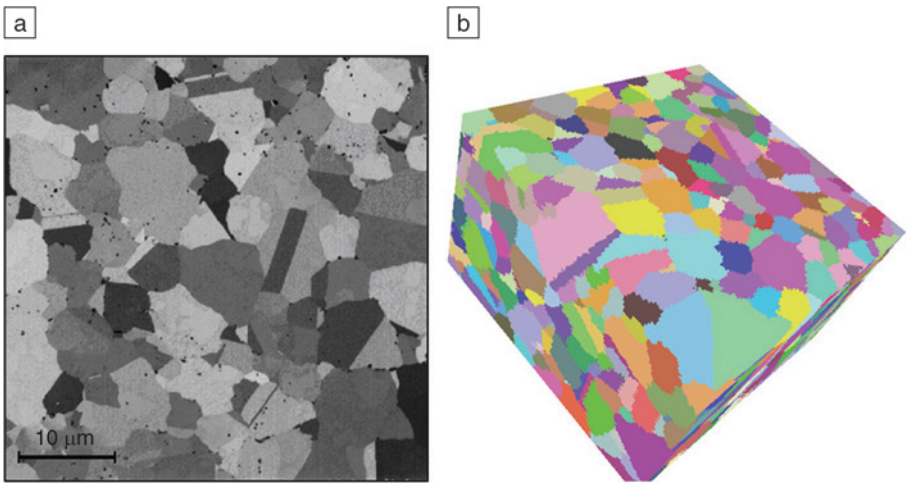


Figure 5. (a) Ion-induced secondary electron image of the IN100 alloy microstructure.[22,23] (b) 3D reconstruction of IN100 created from EBSD data. The dimensions of the parallelepiped volume are 41 × 41 × 29 μm, and the cubic voxel dimension is 0.25 μm.

data files were combined into a 3D array. Voxel data segmentation was performed by measuring the misorientation of neighboring voxels. Voxels were grouped together as grains if the misorientation was below a critical value (4°). Once all sets of contiguous voxels with similar orientation were identified and classified, data cleaning routines were run to refine the quality of the data set. These routines consist of filters for minimum grain size to remove individual erroneous data points, as well as a final alignment procedure to ensure the 3D volume is reconstructed properly. A reconstruction of the 3D volume is shown in Figure 5b, where the dimensions of the volume are 41 × 41 × 29 μm, and each grain is assigned a different color in this image.

One drawback to collecting EBSD data for an FIB tomography experiment is the significant increase in time required for data collection. The time required to collect a 50 × 47 μm EBSD map with a 0.25 μm pixel size at an acquisition rate of 58 points per second was approximately 11 min. By comparison, the other individual steps in the serial sectioning experiment did not take as much time: cross-section milling using a 3000 pA beam (8 min), all sample stage repositioning via pattern matching (6 min), and collection of four ISE images of the same area with a 50 nm pixel size (5 min). The time needed for EBSD data collection was approximately 36% of the cycle time, even though the pixel resolution of the EBSD data was only one-fifth the resolution of image data.

## Comments on Future Developments and Needs

From the examples in the previous sections, it is clear that FIB and FIB–SEM microscopes are capable of high-fidelity characterization of the morphology, crystallography, and chemistry of micron- and submicron-sized features in 3D. Unlike many other tomographic instruments, these microscopes are not optimized solely for this task, as other primary functions, including the production of site-specific TEM lamellae and direct-write micromachining, are possible; these two subjects are the focus of other articles in this issue. One barrier to making FIB tomography more commonplace is that these experiments can require significant time to complete, depending on the volume size that is examined and the type of data that is collected. Although some experiments last less than a few hours, the third example of FIB–EBSD tomography required four days to complete.[22,23] These instruments are typically placed in multiuser facilities and are not usually dedicated to tomography; therefore, an acute need exists for faster data acquisition. Instrument manufacturers continue to do their part by improving the performance of various subsystems, and the latest generation of microscopes features electron and ion columns that have advanced imaging and low-kV milling capabilities, low-drift piezoelectric stages, faster EBSD cameras, and high-count-rate EDS systems. These changes continue to shorten the time needed to complete a serial sectioning experiment and enable more robust experimental data collection.

Although these improvements are welcome, the other aspect of tomographic analysis that requires further development is robust segmentation procedures for the complex multiscale microstructures that are often observed in engineering materials. The transition of advanced signal processing methods to the materials science community will be extremely beneficial, as will the incorporation of multiple data sources within a single tomographic experiment (i.e., data fusion). Similarly, smart or informed acquisition methodologies, where segmentation is performed in real time and feedback is supplied to a microscope as to the type of additional data that needs to be collected to positively identify all microconstituents, should improve the quality of data classification and possibly shorten experimental acquisition time. With these improvements—and as FIB and FIB–SEM microscopes become more widely available in materials laboratories—we envisage that quantitative tomography at the microscale will become a commonplace characterization methodology.

## Acknowledgments

M.D. Uchic acknowledges support from the Materials and Manufacturing Directorate and the Air Force Office of Scientific Research. B. Inkson acknowledges financial support from the Royal Society and the Engineering and Physical Sciences Research Council (EPSRC), United Kingdom.

## References

1. G. Spanos, *Scripta Mater.* **55**, 3 (2006).
2. R.T. DeHoff, *J. Microsc.* **131**, 259 (1983).
3. M.V. Kral, G. Spanos, *Acta Mater.* **47**, 711 (1999).
4. A.C. Lund, P.W. Voorhees, *Acta Mater.* **50**, 2585 (2002).
5. J.E. Spowart, H.M. Mullens, B.T. Puchala, *JOM* **37**, 35 (2003).
6. J.C. Fiala, M. Feinberg, V. Popov, K.M. Harris, *J. Neurosci.* **18** (21), 8900 (1998).
7. B. Foster, *Am. Lab.* **37**, 42 (2005).
8. J. Alkemper, P.W. Voorhees, *Acta Mater.* **49**, 897 (2001).
9. D.J. Rowenhorst, A. Gupta, C.R. Feng, G. Spanos, *Scripta Mater.* **55**, 11 (2006).
10. T. Sakamoto et al., *Jpn. J. Appl. Phys.* **37**, 2051 (1998).
11. D.N. Dunn, R. Hull, *App. Phys. Lett.* **75**, 3414 (1999).
12. M.W. Phaneuf, J. Li, *Proc. Microsc. Microanal.* **6**, 524 (2000).
13. B.J. Inkson, T. Steer, G. Möbus, G.T. Wagner, *J. Microsc.* **201**, 256 (2001).

14. B.J. Inkson, M. Mulvihill, G. Möbus, *Scripta Mater*. **45**, 753 (2001).
15. T.J. Steer et al., *Thin Solid Films* **413**, 147 (2002).
16. L. Holzer et al., *J. Microsc*. **216**, 84 (2004).
17. R.K. Bansai, A. Kubis, R. Hull, J.M. Fitz-Gerald, *J. Vac. Sci. Technol., B* **24**, 554 (2006).
18. J.E. Spowart, *Scripta Mater*. **55**, 5 (2006).
19. P.G. Kotula, M.R. Keenan, J.R. Michael, *Micros. Microanal*. **12**, 36 (2006).
20. N. Zaafarani et al., *Acta Mater*. **54**, 1863 (2006).
21. J. Konrad, S. Zaefferer, D. Raabe, *Acta Mater*. **54**, 1369 (2006).
22. M.D. Uchic, M.A. Groeber, D.M. Dimiduk, J.P. Simmons, *Scripta Mater*. **55** 23 (2006).
23. M.A. Groeber et al., *Mater. Charact*. **57**, 259 (2006).
24. H.Z. Wu, S.G. Roberts, G. Möbus, B.J. Inkson, *Acta Mater*. **51**, 149 (2003).
25. J. Orloff, M. Utlaut, L. Swanson, *High-Resolution Focused Ion Beams: FIB and Its Applications* (Kluwer Academic/Plenum, New York, 2003).
26. M.V. Kral et al., in *ASM Handbook, Volume 9: Metallography, Microstructures* (ASM International, Materials Park, OH, 2004) p. 448.
27. P.M. Nellen, V. Callegari, U. Sennhauser, *Chimia* **60**, 735 (2006).
28. E.L. Principe, in *Focused Ion Beam System: Basics and Applications*, N. Yao, Ed. (Cambridge University Press, Cambridge, UK, 2007) pp. 146–186.
29. FEI Company, *AutoScript Technical Note PN 25564-C* (FEI Company, Hillsboro, OR, 2000).
30. J.R. Russ, *The Image Processing Handbook* (CRC Press, Boca Raton, Florida, ed. 3, 1999).
31. R.C. Gonzales, R.E. Woods, *Digital Image Processing* (Prentice Hall, New Jersey, ed. 2, 2002).
32. E. Lifshin, J. Evertsen, E. Principe, J. Friel, *Proc. 30th Int. Symp. Testing Failure Anal*. (2004) p. 429.
33. R.M. Langford et al., *J. Micromech. Microeng*. **12**, 111 (2002).
34. J. Wilson et al., *Nature Mater*. **51**, 541 (2006).
35. M. Milani, M. Ballerini, F. Squadrini, *Scanning and Force Microscopies for Biomedical Applications II*, E. Tamiya, E.S. Yeung, Eds., *SPIE* **3922** (2000) p. 1605.
36. J.J.L. Mulders, G. Knott, B.H. Lich, *Proc. Microsc. Microanal*. **12**, 1324 CD (2006).
37. L. Tomutsa, V. Radmilovic, *Technical Report LBNL-52648* (Lawrence Berkeley National Laboratory, Berkeley, CA, 2003).
38. Z.H. Xie et al., *J. Mater. Res*. **21**, 2600 (2006).
39. L. Holzer et al., *J. Am. Ceram. Soc*. **89**, 2577 (2006).
40. B. Münch, P. Gasser, L. Holzer, R.J. Flatt, *J. Am. Ceram. Soc*. **89**, 2586 (2006).
41. R. Flatt, P. Bowen, *J. Am. Ceram. Soc*. **89**, 1244 (2006).
42. N.S. Martys, *J. Rheol*. **49**, 401 (2005).
43. D.M. Dimiduk et al., *Materials Processing and Design: Modeling, Simulation and Applications, NUMIFORM 2004,* S. Ghosh, J.M. Castro, J.K. Lee, Eds., (Springer, New York, 2004) p. 1705.
44. A.J. Schwartz, M. Kumar, B.L. Adams, Eds., *Electron Backscatter Diffraction in Materials Science* (Kluwer Academic/Plenum Press, New York, 2000).
45. W. Xu et al., *Mater. Charact*. (2007) in press. □